Eur. Phys. J. D **21**, 97–100 (2002)
DOI: 10.1140/epjd/e2002-00183-2

THE EUROPEAN PHYSICAL JOURNAL D

Relativistic electron beams detection in a dense plasma focus

J. Pouzo[1,a], H. Acuña[2], M. Milanese[1], and R. Moroso[1]

[1] Instituto de Física Arroyo Seco, Universidad Nacional del Centro de la Provincia de Buenos Aires and CONICET, Pinto 399, 7000 Tandil, Argentina
[2] Departamento de Física, Facultad de Ciencias Exactas y Naturales, Universidad Nacional de Mar del Plata, Funes 3350, 7600 Mar del Plata, Argentina

Received 28 February 2002 / Received in final form 7 May 2002
Published online 24 September 2002 – © EDP Sciences, Società Italiana di Fisica, Springer-Verlag 2002

Abstract. Fast electron beams into a hollow anode of a small plasma focus machine (2 kJ, 4 μF) were measured. The diagnostic method designed for this purpose is founded in a small Rogowski coil introduced into a cavity performed in the anode. By means of this, electron beam pulses of about 10 ns width generated in the plasma focus are detected. Simultaneously, hard X-ray signals obtained from a scintillator-photomultiplier system are registered. The electron beam energy was measured through the time-of-flight of the electrons between probe and anode top. The beams are found to be relativistic and its energy is into the range of hard X-rays energy. An analysis of signal intensities and relative delays for three hundred shots are here presented.

PACS. 52.58.Lq Z-pinches, plasma focus and other pinch devices – 52.70.Ds Electric and magnetic measurements – 52.70.Nc Particle measurements

1 Introduction

The plasma focus (DPF) devices generate high temperature (some keV) and high-density (10^{19}–10^{20} cm^{-3}) plasmas that live during very brief times (around 100 ns). In the final stage of the plasma evolution (maximum compression of the column) several disruptions can be observed along the plasma column. The most accepted hypothesis [1–3] is that the necking and subsequent breaking of the column are the consequence of $m = 0$ instabilities. In these points, a charge separation effect can originate fast particle beams as a consequence of the high electric field there generated. Then, an axial ion beam moving away the anode is generated, and a corresponding electron beam of the same energy goes in the opposite sense. The impact of electron beams on the anode produces hard X-ray emission due to the bremsstrahlung effect [4–8] on the metal. On the other hand, the ion beams colliding with the thermal ions in the plasma bulk produce, when deuterium is used as filling gas, beam-target D–D fusion reactions in the focus. Then, the study of ion and electron beams generated in the plasma focus contributes to the basic plasma physics knowledge and also to foreseeable applications. Between them, we can mention nuclear fusion, ion implantation in metals, surface coatings, ultra fast flashes of hard X-ray for biological applications, soft X-rays for lithography, microscopy and laser pumping [9–12], fast neutron pulses for neutrongraphy [13], etc.

[a] e-mail: pouzo@exa.unicen.edu.ar

In this work we detect electron beams by means of a small Rogowski coil and register the hard X-ray emission, correlating them and deriving the energy of the beams. A comparison of the electron beam energy with the deuteron beam energy previously measured in the same device is made. The relation of these measurements with the D–D fusion neutrons emission is made in order to investigate the mechanism that produces nuclear fusion reactions in the focus and to check the hot-spots and charge-separation hypothesis.

2 Experimental systems and methods

In this experiment a Mather-type plasma focus called PACO [14] is used. The capacitor bank charged at 31 kV stores 2 kJ of energy. The peak current is 250 kA and the average neutron yield is 4×10^8 per shot when pure deuterium (D_2) in the range 1–2 mb is used as filling gas. The coaxial electrodes of the experiment are made in brass. The inner one ($\phi_i = 40$ mm, 100 mm long) is hollow; it is the anode at 31 kV in the beginning of the discharge. A brass stopper axially perforated (diameter of the channel: 4 mm, length: 20 mm) is inserted in the anode free end (focus zone). The anode is closed at the top with a polished aluminium plate. The outer electrode ($\phi_o = 110$ mm), at ground, consists of 12 rods. The experimental setup is shown in Figure 1a. The time-integrated measurement of neutrons (Y) is performed with two silver activation counters in side-on position. The time-resolved

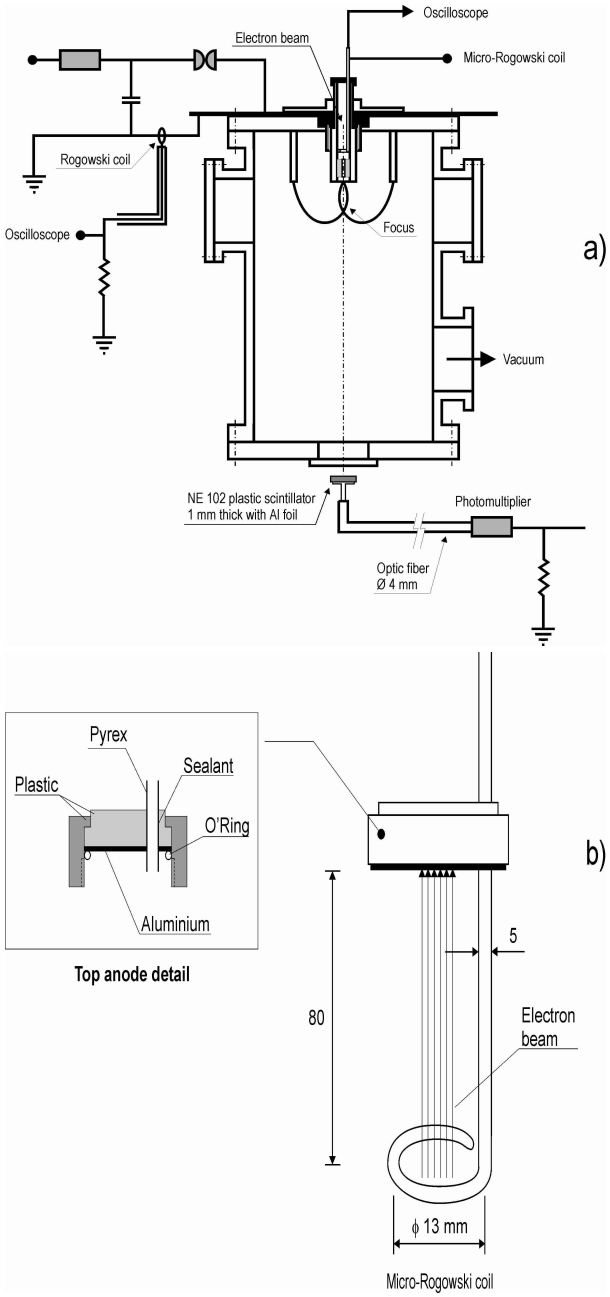

Fig. 1. (a) Experimental setup: discharge chamber, electron beam detector into the cylindrical anode, hard X-ray detector outside the vacuum chamber; (b) probe details.

hard X-ray emission is measured with a fast scintillator-photomultiplier detector. The scintillator, located in end-on position, is very thin (0.5 mm) in order to minimize the interaction with neutrons. The light signal coming from the scintillator is driven, through an optic fiber, to a photomultiplier located into the Faraday cage. A Rogowski coil (response in frequency higher than 100 MHz) in the discharge line registers the total discharge current derivative ($\mathrm{d}I/\mathrm{d}t$).

The X-ray detector is covered with a 100-μm thick aluminium foil to shield it from visible light. It is located

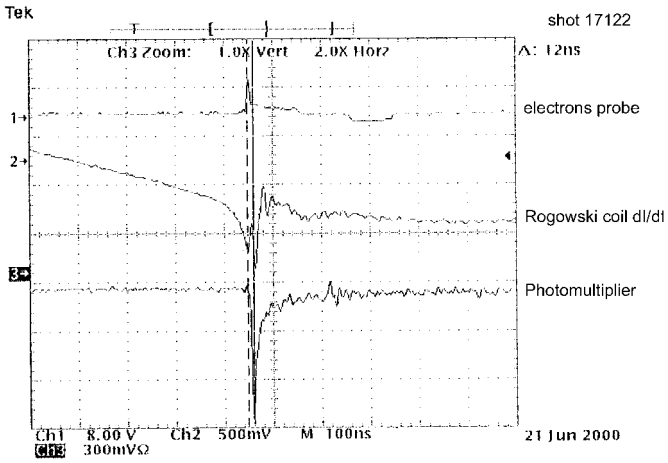

Fig. 2. Oscilloscope traces from the detectors. Upper beam: micro Rogowski coil detecting electron beams; middle: Rogowski coil detecting the total discharge current; lower: scintillator-photomultiplier detecting hard X-ray pulses. The three signals are synchronized.

outside the discharge chamber, in front of a 4-mm thick glass window. This window filters X-rays with energies below 25 keV [15]; then, this is the energy threshold in our hard X-ray measurements.

The current derivative of the electron beams is registered with a small Rogowski coil electron probe located inside of the hollow anode (see Figs. 1a and 1b). The mean diameter of this Rogowski coil is 13 mm. It is very well shielded against the electromagnetic noise by a grounded aluminium foil in suitable geometry, added to the fact that the proper anode constitutes a shielding. It is also electrically well isolated against the very high sinusoidal voltage by means of a Pyrex tube (ϕ_o = 5 mm, 0.7 mm thick) into which the Rogowski coil and its connection cables are housed. The response in frequency of the probe is higher than 100 MHz. There is not any space, practically, between the Pyrex cover and the anode wall. The coil plane is perpendicular to the electrode symmetry axis and it is located at 20 mm from the anode free end leaning on the above-mentioned stopper. The electron beams generated in the focus cross the probe cover an 80-mm path (into the hollow anode) and then impact the inner face of the anode top (made in aluminium) producing hard X-rays pulses.

The main Rogowski coil, electron beam detector and photomultiplier output signals are registered in a Tektronix TDS 540A oscilloscope (500 MHz bandwidth). The delay of each signal produced by the oscilloscope transmission lines (included the optic fiber's delay) was measured and compensated in order to register the events simultaneously with a precision better than 1 ns in the multichannel oscilloscope. The $\mathrm{d}I/\mathrm{d}t$ dip of the Rogowski coil was adopted as reference time. This procedure is justified because this time corresponds to the minimum pinch diameter, as it was studied in a previous work [16]. In Figure 2, a typical oscilloscope screen is shown with hard X-rays, $\mathrm{d}I/\mathrm{d}t$ Rogowski coil and electron probe simultaneous

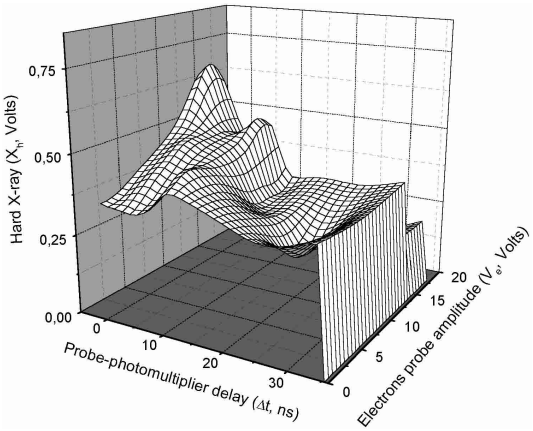

Fig. 3. 3-dimensional graph for the hard X-ray pulse amplitude as a function of electron beam – hard X-ray pulse delay and electron beam pulse amplitude.

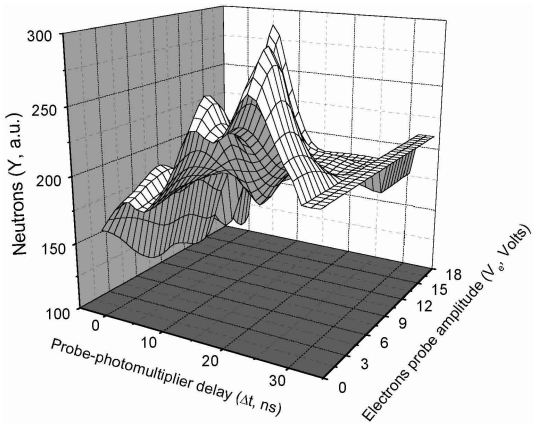

Fig. 4. 3-dimensional graph for the neutron yield as a function of the electron beam amplitude and electron beam – hard X-ray pulse delay.

traces; there is showed the maximum (peak) of each parameter and its relative delay.

3 Results and comments

We measured, in about five hundred discharges, the following magnitudes: time delay between electron-beam and X-ray peaks (Δt), amplitude of X-ray (X_h) and electron beam (V_e) peaks, and the time-integrated neutron yield (Y); the main parameters, filling gas deuterium density and capacitor bank voltage are kept constant. It can be seen in Figure 2 that all the signals have a very low noise level.

In several hundred images of the plasma focus taken with an image converter camera in previous works, by instance those of references [1,16,17], we observed that the pinch column is a pair cm long and its diameter is about 1 mm. Also we never observed it shifted than the centre by more than some millimetre. We have then inferred that most of the e-beams does cross the probe. In a total of several hundred discharges we observed only a low percent of "anomalous" e-beam signals that consist in temporal coincidence between the e-beam detection and X-ray emission. This behaviour could be attributed to the beam impact on the stopper anode surface. We have, then, detached these "anomalous" points from our statistics.

The three variables V_e, X_h and Δt are represented in a three-dimensional graph, as it is shown in Figure 3. In order to construct this graph we rejected a few not much reliable values and put all the data in a table of origin using a "Weighted Average Gridding Method". As it can be observed, both X_h and V_e are higher as shorter is Δt. The speed v of an electron of the beam can be estimated by the distance between the micro-Rogowski coil and the top of the anode (where the hard X-ray are emitted) – delay rate, that is $v = 8$ cm/Δt. The fact that V_e increases when Δt decreases is a logic consequence of the high electron current due to the high values of v. Then, we can deduce that the intensity of X-rays X_h is higher as faster is the electron beam.

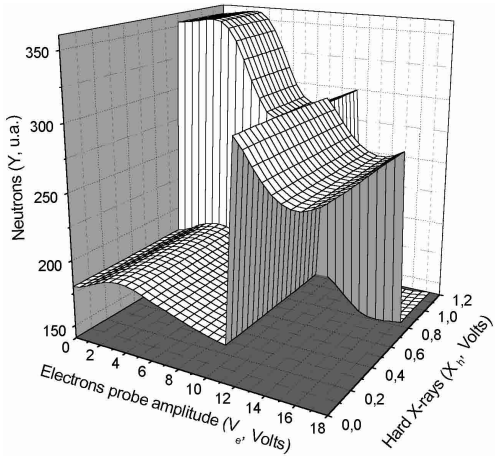

Fig. 5. 3-dimensional graph for the neutron yield as a function of the electron beam and hard X-ray pulse amplitude.

Figure 4 shows that Y has a maximum for $\Delta t \cong 10$ ns and high values of V_e. In Figure 5 it can be seen that Y is high for high values of V_e and X_h, but it is still higher for lower values of V_e. This behaviour of the neutron production respect to the intensity of the electron beam can be considered as not coherent with the hypothesis "high beam intensity corresponds to high neutron production". But just we showed in a previous work [18] that there is a coexistence of thermal and non-thermal mechanisms in the focus, and Y is higher as stronger is each effect, separately or together. In this sense, the results observed in Figures 4 and 5 are coherent with the conclusions got in reference [18].

The values of the measured electron speed v vary between 0.3 and 1×10^{10} cm/s, so that, they are relativistic. Calculating the kinetic energy T according to Einstein's formula: $T = mc^2(\gamma - 1)$, where $\gamma = (1 - v^2/c^2)^{-1/2}$, the range of T results similar to the hard X-rays energy range measured in other DPF devices [5,8], that is, tens of keV.

Figure 6 shows a macro-photography where impacts of electron beams on the hollow anode top inner surface can be observed. This picture was released after a series of

Fig. 6. Photo of the metallic plate at the end of the anode where the impact of electron beams can be observed.

half hundred shots. The surface where the electron beams impact consisted in a polished sheet with 0.9 mm aluminium thick. The purpose of this picture is take measure of the X-rays sources size from the anode surface 0.2 mm micro-impacts. It could be seen also different type of traces related with plasma impacts with about 2 mm diameter.

4 Final remarks

In this work several experimental observations result coincident with previous hypotheses of the plasma focus phenomenon. The fact that the electron velocity is close to the light velocity corresponds to the acceleration in electric fields very higher than the corresponding to the electrical discharge. Then, this result is coherent with the hypothesis of a strong charge separation effect. The fact that the range of electron beam kinetic energy T is into that of hard X-rays [5,8] also reinforces this assumption. On the other hand, the correlation of the neutron production with the electron beam intensity agrees with the hypothesis formulated in previous works. In reference [18], the correlation between hard X-ray intensity and neutron yield (Fig. 7 of Ref. [18]) drove us to conclude that an important part of the fusion reactions is due to beam-target effect. The experimental verification of the existence of axial electron beams (and the consequent existence of axial deuteron beams) made here, correlated with the neutron yield allows also conclude that there is an important part of the fusion reactions originated in beam-target processes. It must be mentioned that the presence of relativistic electron beams was also observed by other authors through other methods [19].

The authors wish to gratefully acknowledge the collaboration of Dr. F. Castillo Mejía to perform the measurements; we thank also the technical assistance of Mrs. E. Szyszkowski, Mr. N. Scali, Mr. C. Santiago and Mr. H. Arislur.

References

1. F. Castillo-Mejía, M. Milanese, R. Moroso, J. Pouzo, J. Phys. D: Appl. Phys. **30**, 1499 (1997)
2. L. Jakubowski, M. Sadowski, E. Baronova, V. Vikhrev, Intern. Symp. Plasma **1**, 121 (1997)
3. J.-P. Rager, *Proc. of the 7th. Eur. Conf. on Contr. Fus. and Pl. Phys.*, Lausanne, 1975, Vol. I, p. 58
4. W.L. Harries, J.H. Lee, D.R. McFarland, Plasma Phys. **39**, 95 (1978)
5. Ch. Maisonnier, F. Pecorella, J.-P. Rager, M. Samuelli, C. Strangio, A. Messina, *5th IAEA Int. Conf. on Pl. Phys. Proc.*, Tokio, 1974, p. 99
6. R.L. Gullickson, R.H. Barlett, Adv. X-ray Anal. **18**, 184 (1975).
7. A. Robledo, I.H. Mitchell, R. Aliaga-Rossel, J.P. Chittenden, A.E. Dangor, M.G. Haines, Phys. Plasma **4**, 490 (1997)
8. H.L.L. van Paassen, R.H. Vandre, R.S. White, Phys. Fluids **13**, 2606 (1970)
9. K. Hirano, H. Kitaoka, J. Phys. Soc. Jap. **65**, 139 (1996).
10. K. Kitaoka, A. Sakurai, T. Yamamoto, K. Shimoda, K. Hirano, J. Phys. Soc. Jap. **64**, 4191 (1995)
11. N. Filippov, T. Filippova, I. Khutoretskia, V. Mialton, V. Vinogradov, Phys. Lett. A **211**, 168 (1996)
12. J. Feugeas, C. Llonch, C. González, G. Galambos, J. Appl. Phys. **64**, 2648 (1988)
13. H. Asia, L. Ueno, Fusion Eng. Des. **7**, 203 (1989)
14. M. Milanese, J. Pouzo, Nucl. Fus. **25**, 840 (1985)
15. J.H. Hubbell, S.M. Seltzer, *Tables of X-Ray Mass Attenuation Coefficients and Mass Energy-Absorption Coeff. from 1 keV to 20 MeV for Elements Z = 1 to 92 and 48 Addit. Substances of Dosimetric Interest*, Ioniz. Radiat. Divis., Phys. Lab., Nat. Inst. of Stands. and Tech., Gaithersburg MD 20899, `http://physics.nist.gov/PhysRefData/XrayMassCoef`
16. M. Milanese, R. Moroso, J. Pouzo, IEEE Trans. Plasma Sci. **21**, 373 (1993)
17. M. Milanese, R. Moroso, J. Pouzo, IEEE Trans. Plasma Sci. **21**, 606 (1993)
18. F. Castillo-Mejía, M. Milanese, R. Moroso, J. Pouzo, J. Phys. D: Appl. Phys. **33**, 141 (2000)
19. L. Jakubowski, M. Sadowski, J. Zebrowski, Nucl. Fus. **41**, 75 (2001)